Rosenthal, Y., Holbourn, A.E., Kulhanek, D.K., and the Expedition 363 Scientists
Proceedings of the International Ocean Discovery Program Volume 363
publications.iodp.org

https://doi.org/10.14379/iodp.proc.363.204.2021

Check for updates

Contents

Data report: refinement of calcareous nannofossil biostratigraphy from the late Oligocene to the Pleistocene, IODP Expedition 363 Hole U1490A[1]

Yvonne Ivy L. Doyongan[2] and Allan Gil S. Fernando[2]

Keywords: International Ocean Discovery Program, IODP, *JOIDES Resolution*, Expedition 363, Western Pacific Warm Pool, Site U1490, biostratigraphy, calcareous nannofossils

Abstract

An Oligocene to recent sedimentary sequence was recovered in Hole U1490A in the northern portion of the Eauripik Rise (western Pacific Ocean) during International Ocean Discovery Program Expedition 363. High-resolution sampling and moderate to good calcareous nannofossil preservation allowed us to adjust the depths for nannofossil events reported shipboard. This study identified 22 zonal boundary markers and 30 secondary calcareous nannofossil events. Because of better preservation of the calcareous nannofossils in the Pliocene–Pleistocene units, more calcareous nannofossil events were observed in that interval than in the older units. In the Miocene units, the discoasters and helicosphaerids (which are important zonal boundary markers) are poorly preserved (fragmented and recrystallized), making it difficult to identify nannofossil zones. In lieu of zonal boundary markers, secondary calcareous nannofossil events were used to refine the biostratigraphy in the Miocene interval.

Introduction

International Ocean Discovery Program (IODP) Site U1490 is located in the northern portion of the Eauripik Rise, which is a north–south trending tectonically stable elevated ridge separating the East and West Caroline Basins. The site is situated at 05°48.95′N, 142°39.27′E at a water depth of 2341 m (Figure **F1**). Three holes were drilled at Site U1490: Holes U1490A, U1490B, and U1490C. Hole U1490A recovered ~380 m of upper Oligocene to recent sediments. Compared to the sediments recovered from other sites cored during Expedition 363, Site U1490 has a relatively low sedimentation rate. The sedimentation rates varied through the recovered intervals and ranged from 0.9 cm/ky in the early to middle Miocene to 5 cm/ky in the late Oligocene, whereas the average sedimentation rate for the whole core was ~1.5 cm/ky. This rate is lower than the rates at nearby sites, including Sites U1488 (~2.5 cm/ky) and U1489 (~2 cm/ky). The sediments from Site U1490 contain calcareous microfossils (nannofossils and foraminifers), siliceous microfossils (radiolarians and diatoms), sponge spicules, clay minerals, and ash. The hole was divided into three subunits (IA, IB, and IC) during shipboard description based on the lithology and composition (i.e., kind of biogenic material, type of clay minerals, and the presence or absence of volcanic ash) (**Rosenthal et al.**, 2018b).

A generalized lithologic log for Site U1490 is shown in Figures **F2** and **F3**. Subunit IA is ~185 m thick and is composed of early Miocene to recent calcareous nannofossil and foraminifer ooze and low amounts of clay minerals and volcanic ash (Figure **F2**). Subunit IB is ~78 m thick and ranges in age from late early to early late Miocene (Figure **F3**). Compared to the previous unit, a significant increase in clay minerals and biosiliceous material was observed in Subunit IB. Subunit IC is a 124 m thick early Oligocene to middle Miocene succession. The siliceous particles that dominate this subunit have distinct dark gray to black indurated layers and nodules and chert fragments (Figure **F3**) (**Rosenthal et al.**, 2018a).

Shipboard calcareous nannofossil biostratigraphic study of core catcher samples (~10 m interval), supplemented in some parts by samples collected from selected sections, recognized 30 calcareous nannofossil events; 15 of these events were zonal boundary markers, and the other 15 were supplementary events. The Pleistocene interval was constrained by 7 calcareous nannofossil events, the Pliocene was constrained by 4 events, the Miocene was constrained by 17 events, and the Oligocene was constrained by 2 events. The top common occurrence of *Cyclicargolithus abisectus*, which has an estimated age of ~24 Ma (Rio et al., 1990; Backman et al., 2012), was found near the base of the hole (**Rosenthal et al.**, 2018a). This study refines the shipboard biostratigraphy of Hole U1490A by examining sediments collected at a higher resolution sampling interval (~1.5 m) of one sample per section.

[1] Doyongan, Y.I.L., and Fernando, A.G.S., 2021. Data report: refinement of calcareous nannofossil biostratigraphy from the late Oligocene to the Pleistocene, IODP Expedition 363 Hole U1490A. *In* Rosenthal, Y., Holbourn, A.E., Kulhanek, D.K., and the Expedition 363 Scientists, *Western Pacific Warm Pool*. Proceedings of the International Ocean Discovery Program, 363: College Station, TX (International Ocean Discovery Program). https://doi.org/10.14379/iodp.proc.363.204.2021
[2] National Institute of Geological Sciences, College of Science, University of the Philippines, Philippines. Correspondence author: **yldoyongan@up.edu.ph**
MS 363-204: Received 2 March 2020 · Accepted 9 September 2020 · Published 5 February 2021

Figure F1. Location of Site U1490.

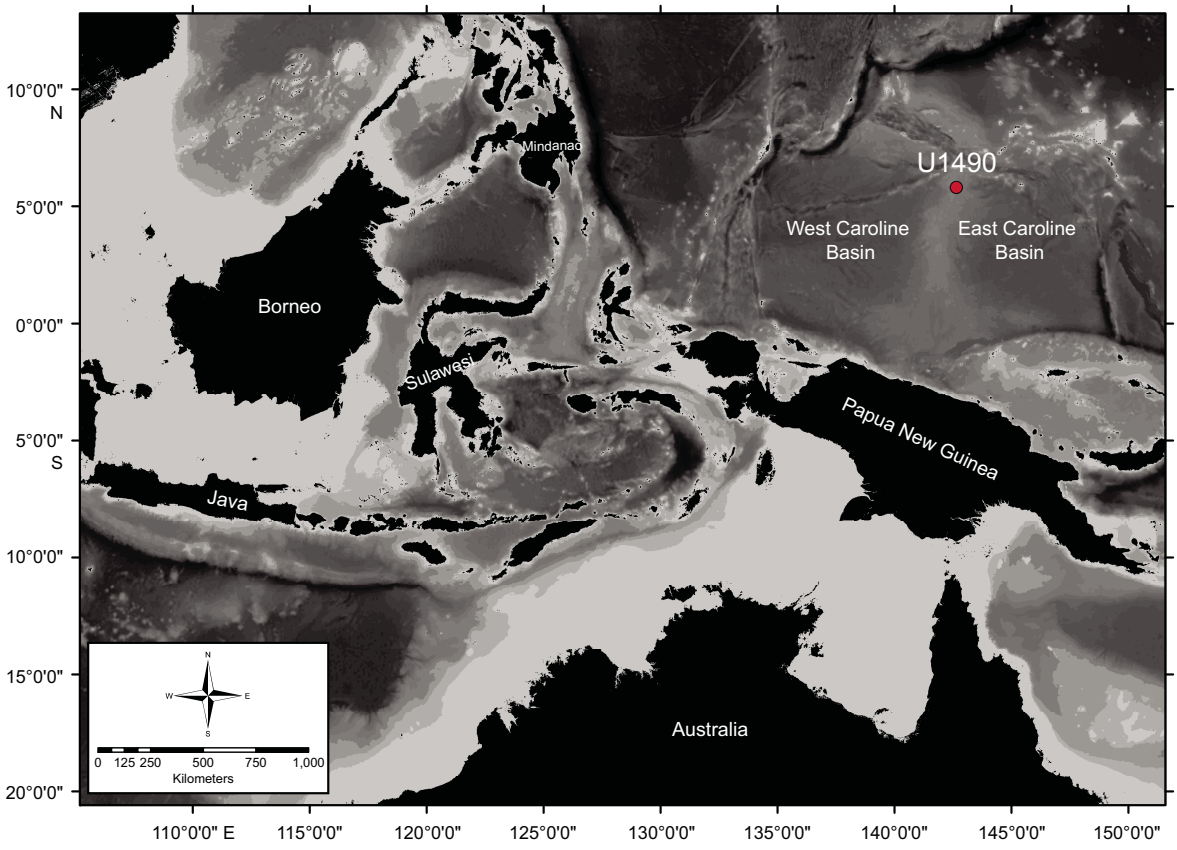

Figure F2. Composite lithologic log of Subunit IA, Holes U1490A–U1490C. Age equivalents, nannofossil zonations, and calcareous nannofossil events (zonal boundary markers and secondary calcareous nannofossil events) observed in this study are also shown. In Hole U1490A, Subunit IA consists of 20 cores extending from late Miocene to recent (from Rosenthal et al., 2018c). T = top, B = base, Bc = base common occurrence, Bpa = base paracme.

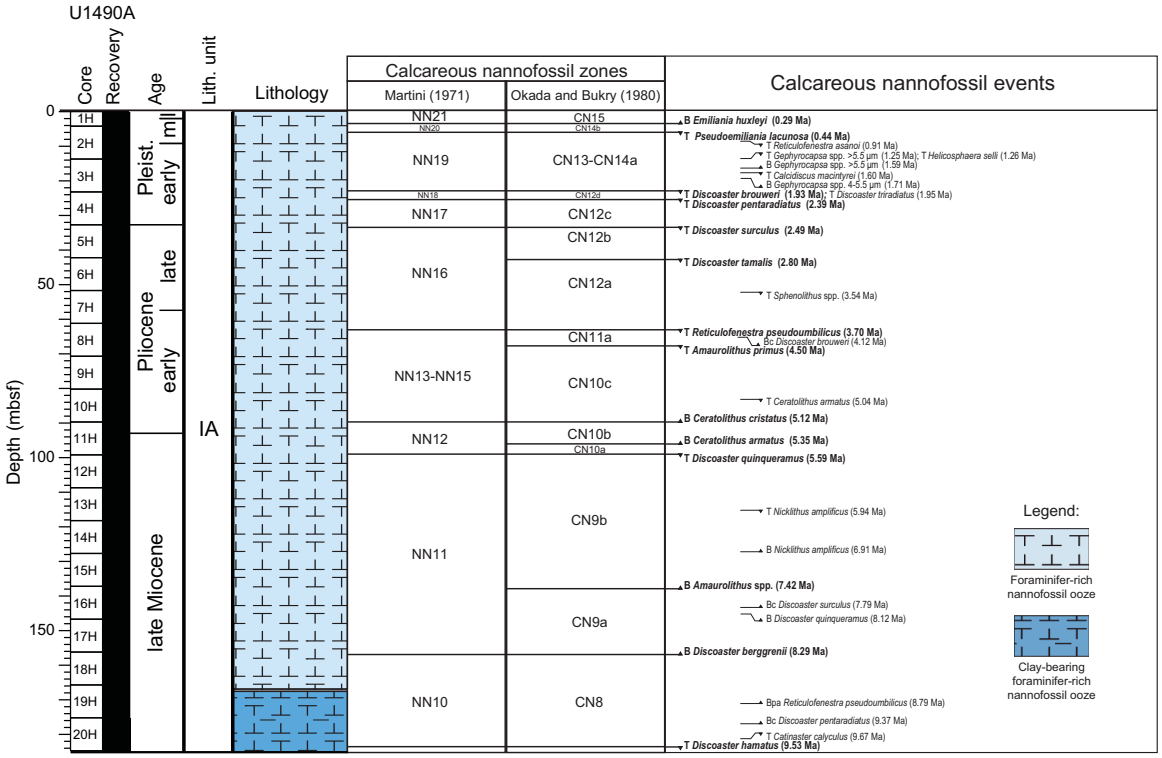

Figure F3. Composite lithologic log of Subunits IB and IC, Holes U1490A–U1490C. Age equivalents, nannofossil zonations, and calcareous nannofossil events (zonal boundary markers and secondary calcareous nannofossil events) observed in this study are also shown. In Hole U1490A, Subunit IB and IC consist of 23 cores extending from late Oligocene to late Miocene (from Rosenthal et al., 2018c). T = top, Tc = top common occurrence, B = base.

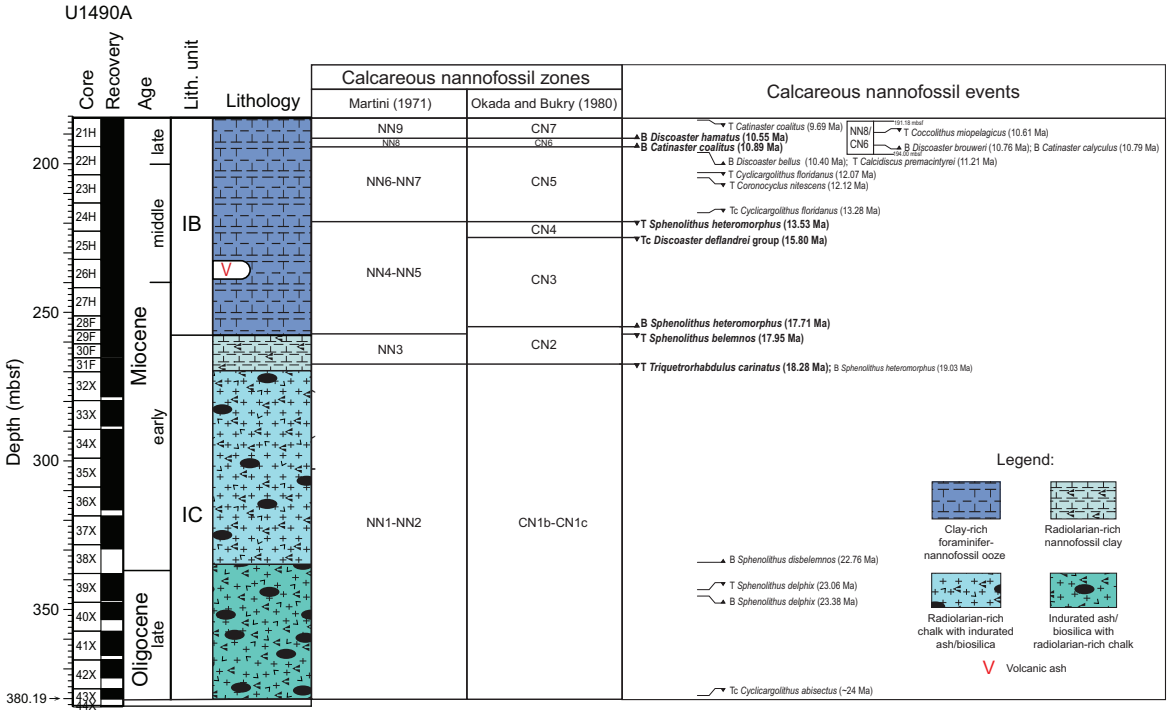

Methodology

The samples were prepared using the standard smear slide preparation technique of Bown and Young (1998). The calcareous nannofossils were examined under an Olympus BX51 polarizing microscope at 1000× magnification in plane-transmitted and cross-polarized light with the occasional use of a quartz wedge compensator. At least 300 fields of view were observed per sample. Calcareous nannofossil taxa were identified to species level if possible using the descriptions provided by the holotypes in Perch-Nielsen (1985) and Aubry (1984a, 1984b, 1984c) and supplemented by the illustrations in Bown (1998) and the guide to the biodiversity and taxonomy Nannotax3 online database (Young et al., 2017). Relative abundances of calcareous nannofossil taxa and degree of preservation were estimated following the same criteria used during Expedition 363 (Table **T1**) (**Rosenthal et al.**, 2018c). Index markers, as well as calcareous nannofossil assemblages, were used to establish the biostratigraphic zonations based on the NP/NN nannofossil zonation scheme of Martini (1971), the CP/CN nannofossil zonation scheme of Okada and Bukry (1980), and the references compiled by **Rosenthal et al.** (2018c). All calcareous nannofossil species identified in the present study are listed in the **Appendix**. Digital images of calcareous nannofossils were taken using a QImaging Go-21 camera attached to the polarizing microscope and the Image ProPlus imaging software.

Table T1. Description of relative abundances and preservation of calcareous nannofossils used in this study. **Download table in CSV format.**

A total of 198 samples were observed in this study (see results in NANNOS in **Supplementary material**). The samples examined were chosen using the calcareous nannofossil shipboard data as reference (Figure **F4**). The shipboard biostratigraphic data identified calcareous nannofossil events based on core catcher samples and a few samples collected from selected sections. The present study examined samples between these intervals to further refine the depth of the nannofossil events and identify additional nannofossil events not observed during the expedition. In the absence of zonal boundary markers, secondary calcareous nannofossil events were used to supplement the biostratigraphic data. Several calcareous nannofossil events were considered:

- T = top.
- Tc = top common occurrence.
- B = base.
- Bc = base common occurrence.
- Bpa = base paracme.

Figure F4. Calcareous nannofossil index markers observed, Hole U1490A. Scale bars = 5 µm. A. *Amaurolithus primus* (4H-6, 117–118 cm). B. *Calcidiscus macintyrei* (4H-5, 98–99 cm). C. *Calcidiscus premacintyrei* (23H-1, 98–99 cm). D. *Catinaster calyculus* (21H-2, 148–149 cm). E. *Catinaster coalitus* (19H-5, 98–99 cm). F. *Ceratolithus armatus* (4H-5, 98–99 cm). G. *Ceratolithus cristatus* (3H-4, 48–49 cm). H. *Coccolithus miopelagicus* (39X-1, 98–99 cm) I. *Coronocyclus nitescens* (36X-CC). J. *Cyclicargolithus floridanus* (39X-1, 98–99 cm). K. *Discoaster bellus* (17H-6, 137–138 cm). L. *Discoaster berggrenii* (16H-CC). M. *Discoaster brouweri* (20H-1, 98–99 cm). N. *Discoaster deflandrei* (29F-2, 148–149 cm). O. *Discoaster hamatus* (20H-CC). P. *Discoaster pentaradiatus* (4H-3, 98–99 cm). Q. *Discoaster quinqueramus* (16H-5, 98–99 cm). R. *Discoaster surculus* (16H-4, 148–149 cm). S. *Discoaster tamalis* (6H-1, 98–99 cm). T. *Discoaster triradiatus* (19H-4, 148–149 cm). U. *Emiliania huxleyi* (1H-1, 0–1 cm). V. *Gephyrocapsa* spp. (<4 µm) (1H-1, 0–1 cm). W. *Gephyrocapsa* spp. (4–5.5 µm) (1H-2, 48–49 cm). X. *Gephyrocapsa* spp. (>5.5 µm) (2H-7, 75–76 cm). Y. *Helicosphaera sellii* (3H-5, 98–99 cm). Z. *Nicklithus amplificus* (13H-CC). AA. *Pseudoemiliania lacunosa* (2H-4, 148–149 cm). AB. *Reticulofenestra asanoi* (2H-6, 139–140 cm). AC. *Reticulofenestra pseudoumbilicus* (23H-CC). AD. *Sphenolithus abies* (29F-CC). AE. *Sphenolithus belemnos* (30F-2, 48–49 cm). AF. *Sphenolithus delphix* (40X-4, 48–49 cm). AG. *Sphenolithus disbelemnos* (38X-1, 98–99 cm). AH. *Sphenolithus heteromorphus* (27H-3, 98–99 cm). AI. *Triquetrorhabdulus carinatus* (31F-CC).

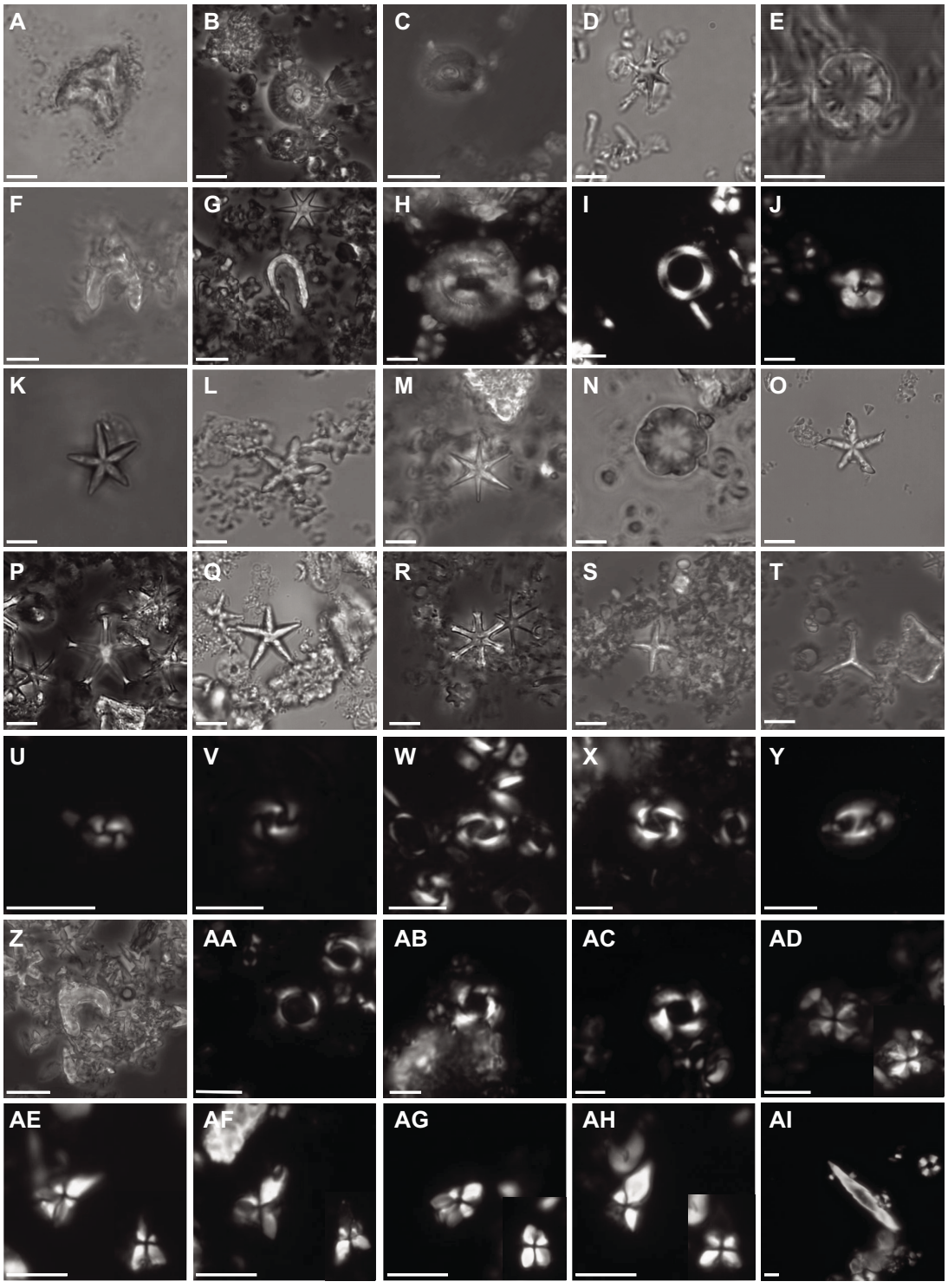

Results

A total of 52 calcareous nannofossil events were identified in this study: 22 were zonal boundary markers, and 30 were secondary calcareous nannofossil events. Generally, the calcareous nannofossils observed were well preserved, especially in the Pliocene–Pleistocene interval. However, in the Miocene sediments, the larger calcareous nannofossils such as the discoasters and ceratoliths were noticeably recrystallized and much more fragmented. As demonstrated by the thickening arm widths and narrowing arm spaces of the discoasters, recrystallization was much more evident in the Oligocene sediments. Therefore, it was difficult to identify the specimens to species level. The results were divided into four sections: Pleistocene, Pliocene, Miocene, and Oligocene. In each section, the zonal boundary markers were given emphasis, whereas the secondary events were briefly mentioned to supplement the establishment of the zonations. The reliability of selected index markers is described in this study based on published literature and recent zonation scheme references.

Pleistocene

The Pleistocene interval was constrained by 12 calcareous nannofossil events: 5 zonal boundary markers and 7 secondary calcareous nannofossil events (Table **T2**). Most of the calcareous nannofossils observed in the Pleistocene interval were placoliths, helicoliths, and discoasters with good preservation and minimal traces of recrystallization or etching. This interval was characterized by the high diversity of species observed, likely due to the good preservation. Gephyrocapsids were prominent in the Pleistocene interval. Following Raffi et al. (1993), appearance and extinction events based on their size variations were used as secondary calcareous nannofossil events (small = <4 µm, medium = 4–5.5 µm, and large = >5.5 µm). All of the nannofossil zones in the NN zonation scheme of Martini (1971) and CN zonation scheme of Okada and Bukry (1980) were clearly identified in this interval.

Biohorizon base *Emiliania huxleyi* (0.29 Ma; base of Zone NN21/CN15) was observed between Samples 363-U1490A-1H-2, 92–93 cm, and 1H-CC (3.92–4.18 meters below seafloor [mbsf]). The base of Zone NN20/CN14b, marked by biohorizon top *Pseudoemiliania lacunosa* (0.44 Ma), was observed between Samples 1H-CC and 2H-1, 96–97 cm (4.18–5.16 mbsf). The base of Zone NN19/CN13–CN14a was marked by biohorizon top *Discoaster brouweri* (1.93 Ma) between Samples 3H-6, 48–49 cm, and 3H-6, 139–140 cm (21.68–22.59 mbsf). In Zone NN19, several secondary calcareous nannofossil events were observed:

- Biohorizon top *Reticulofenestra asanoi* (0.91 Ma) between Samples 2H-2, 48–49 cm, and 2H-3, 98–99 cm (6.18–8.18 mbsf);
- Biohorizon top *Gephyrocapsa* spp. (>5.5 µm; 1.25 Ma) between Samples 2H-6, 139–140 cm, and 2H-7, 75–76 cm (13.09–13.95 mbsf);
- Biohorizon top *Helicosphaera sellii* (1.26 Ma) between Samples 2H-6, 139–140 cm, and 2H-7, 75–76 cm (13.09–13.95 mbsf);
- Biohorizon base *Gephyrocapsa* spp. (>5.5 µm; 1.59 Ma) (Backman et al., 2012) between Samples 3H-2, 48–49 cm, and 3H-2, 148–149 cm (15.68–16.68 mbsf);
- Biohorizon top *Calcidiscus macintyrei* (1.60 Ma) between Samples 3H-2, 148–149 cm, and 3H-3, 98–99 cm (16.68–17.68 mbsf); and
- Biohorizon base *Gephyrocapsa* spp. (4–5.5 µm; 1.71 Ma) (Backman et al., 2012) between Samples 3H-4, 48–49 cm, and 3H-5, 48–49 cm (18.68–20.18 mbsf).

Table T2. Comparison of Pliocene–Pleistocene calcareous nannofossil biohorizons reported in shipboard results and this study, Hole U1490A. **Download table in CSV format.**

Biohorizon top *H. sellii* was observed to be coincident with biohorizon top *Gephyrocapsa* spp. (>5.5 µm).

Young (1991) noted that *Gephyrocapsa* spp. (<4 µm) has two acme events in the Pleistocene interval. The first acme event was noted in Zone NN19, and the second acme event was observed near the boundary between Zones NN20 and NN21. These acme events were also observed in the sediments from Hole U1490A, although the boundaries were quite unclear because of the generally high abundance of *Gephyrocapsa* spp. (<4 µm). In Zone NN19, the base and top acme of the first event were observed between Samples 363-U1490A-3H-1, 98–99 cm, and 3H-2, 48–49 cm (14.68–15.68 mbsf), and between Samples 2H-2, 48–49 cm, and 2H-3, 98–99 cm (6.18–8.18 mbsf), respectively. The base acme of the second event was between Samples 2H-1, 96–97 cm, and 2H-2, 48–49 cm (5.16–6.18 mbsf), and the top acme was between Samples 1H-1, 0–1 cm, and 1H-2, 48–49 cm (0–1.98 mbsf). The boundary between Zones NN20 and NN21 was within the range of the second acme event, which was consistent with the observation of Young (1991). These two acme events are not shown in Table **T2**.

The base of Zone NN18/CN12d was marked by biohorizon top *Discoaster pentaradiatus* (2.39 Ma) between Samples 363-U1490A-4H-1, 98–99 cm, and 4H-2, 48–49 cm (24.18–25.18 mbsf). Biohorizon top *Discoaster triradiatus* (1.95 Ma) was observed in Zone NN18 between Samples 3H-6, 48–49 cm, and 3H-6, 139–140 cm (21.68–22.59 mbsf). Biohorizon top *D. brouweri* was observed to be coincident with biohorizon top *D. triradiatus*. The base of Zone NN17/CN12c was marked by biohorizon top *Discoaster surculus* (2.49 Ma) between Samples 4H-CC and 5H-1, 98–99 cm (33–33.68 mbsf). This event was also near the Pliocene/Pleistocene boundary and was used to approximate the position of the boundary at ~34 mbsf.

Among the zonal boundary markers used in this study, biohorizon base *E. huxleyi*, biohorizon top *P. lacunosa*, and biohorizon top *D. brouweri* were reported to have high reliability with clear appearance/extinction events that are globally synchronous (Raffi et al., 2006). Thierstein et al. (1977) and Gartner (1977) first reported the high reliability of biohorizon base *E. huxleyi* and biohorizon top *P. lacunosa*. These datums were retained in the recent zonation scheme of Backman et al. (2012). Biohorizon top *D. pentaradiatus* and biohorizon top *D. surculus* were given a lower reliability rank by Raffi et al. (2006). In Backman et al. (2012), biohorizon top *D. pentaradiatus* was used as a zonal boundary marker but biohorizon top *D. surculus* was used as a secondary calcareous nannofossil event.

Pliocene

The Pliocene interval was constrained by 7 calcareous nannofossil events, 4 of which were zonal boundary markers and 3 of which were secondary calcareous nannofossil events (Table **T2**). Similar to the Pleistocene interval, most of the calcareous nannofossils identified were placoliths, helicoliths, and discoasters, with the addition of ceratoliths and sphenoliths. Calcareous nannofossils were generally moderately preserved in this interval, although most discoasters and ceratoliths appear to be overgrown/affected by recrystallization. Despite the lower degree of preservation in the Pliocene interval than in the Pleistocene, nannofossil diversity was still high because of the presence of more *Discoaster* species. All of the nannofossil zones in Martini (1971) and Okada and Bukry (1980)

were identified or clearly delineated except for Zones NN14/CN11b and NN15.

The base of Zone NN16/CN12a was marked by biohorizon top *Reticulofenestra pseudoumbilicus* (>7 µm; 3.70 Ma) between Samples 363-U1490A-8H-1, 98–99 cm, and 8H-2, 48–49 cm (62.18–63.18 mbsf). In Zone NN16, several nannofossil events were recognized:

- Biohorizon top *Discoaster tamalis* (2.80 Ma) between Samples 5H-7, 57–58 cm, and 5H-CC (41.98–42.13 mbsf), which marked the lower boundary of Subzone CN12b; and
- Biohorizon top *Sphenolithus* spp. (3.54 Ma) between Samples 6H-CC and 7H-1, 98–99 cm (51.88–52.68 mbsf).

The markers for the base of Zones NN15 and NN14/CN11b (i.e., biohorizon top *Amaurolithus tricorniculatus* and biohorizon base common *Discoaster asymmetricus*, respectively) were not observed in the present study; however, biohorizon base common *D. brouweri* (4.12 Ma) occurred in this zone between Samples 8H-2, 148–149 cm, and 8H-3, 98–99 cm (64.18–65.18 mbsf). This event occurred just above biohorizon base common *D. asymmetricus* (**Rosenthal et al.**, 2018a). The base of Zone NN13/CN10c was marked by biohorizon base *Ceratolithus cristatus* (5.12 Ma) between Samples 10H-6, 48–49 cm, and 10H-7, 71–72 cm (88.18–89.91 mbsf). The following nannofossil events were found in this zone:

- Biohorizon top *Amaurolithus primus* (4.50 Ma), which marks the base of Subzone CN11a between Samples 8H-3, 98–99 cm, and 8H-4, 148–149 cm (65.18–67.18 mbsf); and
- Biohorizon top *Ceratolithus armatus* (5.04 Ma) between Samples 10H-2, 48–49 cm, and 10H-3, 96–97 cm (82.18–84.16 mbsf).

Biohorizon base *C. cristatus* was the event nearest the Miocene/Pliocene boundary, which is located at ~90 mbsf.

Among the zonal boundary markers, biohorizon top *R. pseudoumbilicus* (>7 µm) is considered a highly reliable marker (Raffi et al., 2006) because of its wide distribution, synchroneity across basins, and well-documented extinction (Backman and Shackleton, 1983; Rio et al., 1990). Biohorizon top *D. tamalis* was given a low reliability rank by Raffi et al. (2006) because of its low abundance and diachroneity across basins. Biohorizon base *C. cristatus* was given a very low reliability rank (Raffi et al., 2006) but still was included in the zonation scheme by Backman et al. (2012) as a secondary calcareous nannofossil event. The low rank was due to the low abundance and sparse distribution of the species (Raffi and Flores, 1995; Backman and Raffi, 1997). Biohorizon top *A. primus* was not assessed in Raffi et al. (2006) but was included in the zonation scheme by Backman et al. (2012) as a secondary calcareous nannofossil event. The distribution of *A. primus* has been noted to be sporadic and rare in several basins, which made it a less reliable marker (Backman and Shackleton, 1983; Rio et al., 1990).

Miocene

The Miocene interval was constrained by 30 calcareous nannofossil events: 13 zonal boundary markers and 17 secondary calcareous nannofossil events (Table **T3**). Most of the calcareous nannofossils observed were placoliths, discoasters, ceratoliths, and sphenoliths. Unlike the Pliocene–Pleistocene interval, the calcareous nannofossils in the Miocene interval have noticeably poorer preservation and therefore lower species diversity. This was especially observed in the large nannoliths (discoasters and ceratoliths), which were mostly overgrown and recrystallized. The helicosphaerids observed in this interval were also overgrown and recrystallized and therefore were not identified to species level. Thus, in zones where a helicosphaerid was a boundary marker, secondary calcareous nannofossil events were used to approximate the boundaries of the zone. Nannofossil zones not clearly identified in the present study were Zones NN1/CN1b, NN2/CN1c, NN5/CN4, NN7/CN5b, and CN8b (Martini, 1971; Okada and Bukry, 1980).

Table T3. Comparison of late Oligocene–Miocene calcareous nannofossil biohorizons reported in shipboard results and this study, Hole U1490A. **Download table in CSV format.**

The base of Zone NN12/CN10a was marked by biohorizon top *Discoaster quinqueramus* (5.59 Ma) between Samples 363-U1490A-11H-6, 48–49 cm, and 11H-6, 138–139 cm (97.68–98.58 mbsf). Biohorizon base *C. armatus* (5.35 Ma) occurred in Zone NN12 between Samples 11H-4, 48–49 cm, and 11H-4, 148–149 cm (94.68–95.68 mbsf), which marked the base of Zone CN10b. The base of Zone NN11/CN9a was biohorizon base *Discoaster berggrenii* (8.29 Ma) between Samples 17H-6, 137–138 cm, and 17H-7, 67–68 cm (155.57–156.37 mbsf). Biohorizon base *Amaurolithus* spp. (7.42 Ma), which marks the base of Zone CN9b, occurred in Zone NN11 between Samples 15H-CC and 16H-1, 48–49 cm (137.57–137.68 mbsf). Several secondary nannofossil events were observed in Zone NN11:

- Biohorizon top *Nicklithus amplificus* (5.94 Ma) between Samples 13H-4, 148–149 cm, and 13H-5, 98–99 cm (114.68–115.68 mbsf);
- Biohorizon base *N. amplificus* (6.91 Ma) between Samples 14H-6, 48–49 cm, and 14H-6, 134–135 cm (126.18–127.04 mbsf);
- Biohorizon base common *D. surculus* (7.79 Ma) between Samples 16H-4, 148–149 cm, and 16H-5, 98–99 cm (143.18–144.18 mbsf); and
- Biohorizon base *D. quinqueramus* (8.12 Ma) between Samples 16H-5, 98–99 cm, and 16H-6, 48–49 cm (144.18–145.18 mbsf).

The base of Zone NN10/CN8 was denoted by biohorizon top *Discoaster hamatus* (9.53 Ma) between Samples 363-U1490A-20H-5, 98–99 cm, and 20H-6, 48–49 cm (182.18–183.18 mbsf). The following secondary calcareous nannofossil events were found in this zone:

- Biohorizon base paracme *R. pseudoumbilicus* (>7 µm; 8.79 Ma) between Samples 19H-4, 48–49 cm, and 19H-5, 98–99 cm (170.68–172.68 mbsf);
- Biohorizon base common *D. pentaradiatus* (9.37 Ma) between Samples 20H-1, 98–99 cm, and 20H-2, 48–49 cm (176.18–177.18 mbsf); and
- Biohorizon top *Catinaster calyculus* (9.67 Ma) between Samples 20H-4, 148–149 cm, and 20H-5, 98–99 cm (181.18–182.18 mbsf).

The base of Zone NN9/CN7 was indicated by biohorizon base *D. hamatus* (10.55 Ma) between Samples 363-U1490A-21H-4, 148–149 cm, and 21H-5, 98–99 cm (190.68–191.68 mbsf). There was an observed reversal in the stratigraphic position of biohorizon top *C. calyculus* and biohorizon top *D. hamatus*. Instead of occurring in Zone NN9, biohorizon top *C. calyculus* was noted in this study in Zone NN10, near the extinction of *D. hamatus*. Biohorizon top *Catinaster coalitus* (9.69 Ma) was observed in Zone NN9 between Samples 20H-CC and 21H-1, 98–99 cm (184.93–185.68 mbsf). The base of Zone NN8/CN6 was marked by biohorizon base *C. coalitus* (10.89 Ma) between Samples 21H-6, 139–140 cm, and 21H-7, 71–

72 cm (193.59–194.41 mbsf). Secondary nannofossil events in Zone NN8/CN6 included the following:

- Biohorizon top *Coccolithus miopelagicus* (10.61 Ma) between Samples 21H-5, 98–99 cm, and 21H-6, 48–49 cm (191.68–192.68 mbsf);
- Biohorizon base *D. brouweri* (10.76 Ma) between Samples 21H-6, 48–49 cm, and 21H-6, 139–140 cm (192.68–193.59 mbsf); and
- Biohorizon base *C. calyculus* (10.79 Ma) between Samples 21H-6, 48–49 cm, and 21H-6, 139–140 cm (192.68–193.59 mbsf).

In Zone NN8, biohorizon base *C. calyculus* and biohorizon base *D. brouweri* were observed in the same sample interval.

The base of Zone NN7/CN5b was marked by biohorizon base common *Discoaster kugleri* (11.90 Ma). Unfortunately, because of poor preservation of the discoasters in the Miocene interval, this species was not identified. Instead, biohorizon top *Cyclicargolithus floridanus* (12.07 Ma) was used to estimate the base of Zone NN7/CN5b between Samples 363-U1490A-22H-6, 49–50 cm, and 22H-7, 66–67 cm (202.19–203.86 mbsf). In this zone, the secondary events biohorizon base *Discoaster bellus* (10.40 Ma) and biohorizon top *Calcidiscus premacintyrei* (11.21 Ma) both occurred between Samples 21H-7, 71–72 cm, and 21H-CC (194.41–194.62 mbsf). Biohorizon base *D. bellus* was a secondary nannofossil event in Zone NN9 (**Rosenthal et al.**, 2018a).

Biohorizon top *Sphenolithus heteromorphus* (13.53 Ma), observed between Samples 363-U1490A-24H-4, 148–149 cm, and 24H-5, 98–99 cm (219.18–220.18 mbsf), was used to mark the base of Zone NN6/CN5a. Biohorizon top *Coronocyclus nitescens* (12.12 Ma) between Samples 23H-1, 98–99 cm, and 23H-2, 48–49 cm (204.68–205.68 mbsf), and biohorizon top common *C. floridanus* (13.28 Ma) between Samples 24H-2, 148–149 cm, and 24H-3, 98–99 cm (216.18–217.18 mbsf), were observed in this zone. As noted in the shipboard nannofossil biostratigraphy data, the base of Zone NN5 using biohorizon top *Helicosphaera ampliaperta* (14.90 Ma) was not observed in this study. No secondary calcareous nannofossil events were reported in Zone NN5. The base of Zone NN4 was identified using biohorizon top *Sphenolithus belemnos* (17.95 Ma) between Samples 29F-1, 98–99 cm, and 29F-2, 48–49 cm (256.88–257.88 mbsf). In Zone NN4, two zonal markers used in the CN zonation scheme by Okada and Bukry (1980) were observed:

- Biohorizon top common *Discoaster deflandrei* group (15.80 Ma) between Samples 25H-1, 98–99 cm, and 25H-2, 48–49 cm (223.68–224.68 mbsf), which marked the base of Zone CN4; and
- Biohorizon base *S. heteromorphus* (17.71 Ma) between Samples 28F-3, 98–99 cm, and 28F-4, 60–61 cm (255.18–255.88 mbsf), which marked the base of Zone CN3.

The base of Zone NN3 was marked by biohorizon top *Triquetrorhabdulus carinatus* (18.28 Ma) between Samples 363-U1490A-31F-2, 48–49 cm, and 31F-2, 148–149 cm (267.28–268.28 mbsf). Coincident with biohorizon top *T. carinatus* was biohorizon base *S. belemnos* (19.03 Ma), which marked the base of Zone CN2. The base of Zone NN2 was reported in Martini (1971) to be marked by biohorizon base *Discoaster druggii* (22.82 Ma). Unfortunately, in both shipboard analysis and in the present study, it was not identified/observed. However, a supplementary calcareous nannofossil event was observed in Zone NN2: biohorizon base *Sphenolithus disbelemnos* (22.76 Ma) between Samples 38X-CC and 39X-1, 98–99 cm (329.49–338.88 mbsf).

Among the Miocene zonal boundary markers, biohorizon base *C. armatus*, biohorizon top *D. quinqueramus*, and biohorizon base *Amaurolithus* spp. were considered reliable markers by Raffi et al. (2006) and were also used as zonal boundary markers in the recent zonation scheme of Backman et al. (2012). Biohorizon base *D. berggrenii* was also used as a zonal boundary marker in Backman et al. (2012) but was ranked low in terms of reliability (Raffi et al., 2006). There was difficulty in determining biohorizon base *D. berggrenii* because of its evolution from *D. bellus*. The difference is the distinct central knob in *D. berggrenii*, which can be difficult to observe in overgrown specimens (Backman and Raffi, 1997). Biohorizon top and base *D. hamatus* were also used as zonal boundary markers in Backman et al. (2012) but were given a low reliability rank (Raffi et al., 2006). This was due to its low abundance, sporadic occurrence (Backman and Raffi, 1997), and diachroneity between low- and mid-latitude sediments (Raffi et al., 1995). Similar to the previously mentioned zonal boundary markers, biohorizon base *C. coalitus* and biohorizon top *S. heteromorphus* were also given a low reliability rank in Raffi et al. (2006). Despite the low rank, both were used as zonal boundary markers in the zonation scheme of Backman et al. (2012). The low reliability rank of biohorizon base *C. coalitus* resulted from the presence of transitional morphotypes from *Discoaster micros* believed to be its ancestor (Raffi et al., 1998), which made recognition of the event difficult. It was also reported by Raffi et al. (1995) that *C. coalitus* could be influenced by ecological conditions resulting in inconsistency in its presence across different basins, which was also postulated for biohorizon top *S. heteromorphus* (Olafsson, 1989; Backman and Raffi, 1997).

Biohorizon top common *D. deflandrei* group was not assessed in terms of reliability in Raffi et al. (2006) but was used in Backman et al. (2012) as a secondary calcareous nannofossil event. Biohorizon base *S. heteromorphus* and biohorizon top *S. belemnos* were used in the zonation scheme of Backman et al. (2012) as a zonal boundary marker and as a secondary calcareous nannofossil marker, respectively. The use of biohorizon base common *S. heteromorphus* was suggested by several studies (Olafsson, 1989; Fornaciari and Rio, 1996; Raffi et al., 2016) because the increase in abundance of the species was much easier to document than its initial appearance in the fossil record. Rather than biohorizon top *T. carinatus*, biohorizon top common *T. carinatus* was used as a zonal boundary marker in Backman et al. (2012). *T. carinatus* was reported to have a sporadic occurrence near its biohorizon top, which made it difficult to determine the exact extinction event, hence its low reliability (Fornaciari and Rio, 1996; Backman et al., 2012).

Oligocene

The upper Oligocene units recovered from Hole U1490A were constrained by biohorizon top and base *Sphenolithus delphix* (23.06–23.38 Ma) between Samples 363-U1490A-39X-4, 148–149 cm, and 39X-5, 98–99 cm (343.88–344.88 mbsf), and between Samples 40X-CC and 41X-1, 98–99 cm (353.26–358.38 mbsf), respectively (Table **T3**). Similar to the Miocene interval, the calcareous nannofossils observed were mostly placoliths, discoasters, and sphenoliths. The placoliths and sphenoliths showed good preservation, whereas the discoasters were highly overgrown and recrystallized. Identification of discoasters to species level in the Oligocene interval was difficult. Biohorizon top common *C. abisectus* (~24 Ma) was observed between Samples 43X-2, 116–117 cm, and 43X-3, 54–55 cm (379.36–379.94 mbsf), near the bottom of the hole and could therefore be used to approximate the age of the oldest sedi-

Figure F5. Age-depth model using all calcareous nannofossil biohorizons identified in this study, Hole U1490A. See Figures F2 and F3 for lithology key. See Tables T2 and T3 for calcareous nannofossil events corresponding to numbers.

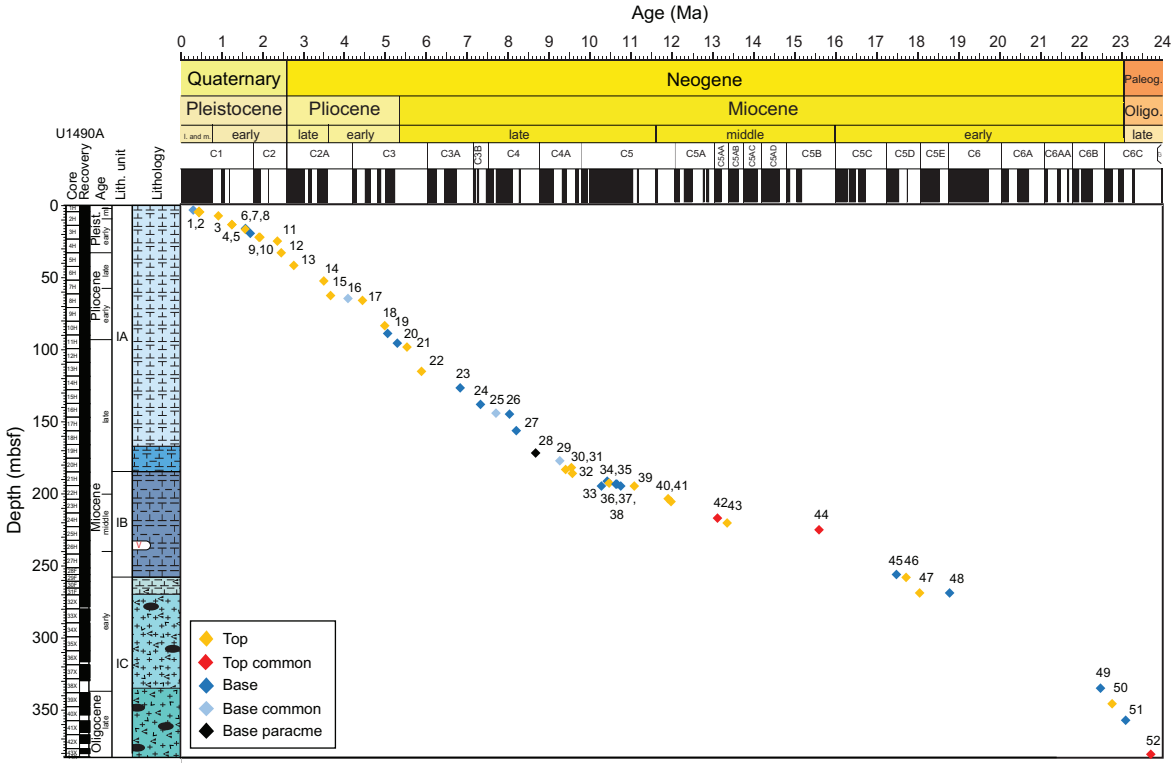

ments recovered in Hole U1490A. The nearest calcareous nannofossil event to the Oligocene/Miocene boundary was biohorizon top *S. delphix*, which was used to estimate the depth of the Oligocene/Miocene boundary at ~344 mbsf.

Age-depth model

Figure **F5** shows the age-depth model for Hole U1490A based on all the calcareous nannofossil events identified between 0.29 Ma (biohorizon base *E. huxleyi*) and 24 Ma (biohorizon top common *C. abisectus*). The sedimentation rates were highest in the Oligocene to early early Miocene interval at 3.67 cm/ky, decreasing to 1.58 cm/ky in the early to middle middle Miocene interval from 334 to 224 mbsf. A continued decrease in the sedimentation rate to 0.94 cm/ky occurred from the middle middle to early late Miocene from 224 to 172 mbsf, and then an increase to 2.15 cm/ky occurred from 172 to 25 mbsf in the late Miocene to early Pleistocene interval. For the rest of the Pleistocene, above 25 mbsf, the sedimentation rate was 1.11 cm/ky. The middle middle to early late Miocene interval had the lowest sedimentation rate in Hole U1490A and was also the interval where several events were either reversed or observed occurring in the same sample interval.

Acknowledgments

We would like thank the International Ocean Discovery Program (IODP) for allowing us to further study the samples obtained from IODP Expedition 363. We would also like to thank the Nannoworks Laboratory of the National Institute of Geological Sciences, University of the Philippines for providing the support and resources needed to finish the analysis. Lastly, to the reviewers of this data report, Dr. Mariem Saavedra-Pellitero and Dr. Denise K. Kulhanek, thank you for giving us invaluable feedback for the improvement of this report.

References

Aubry, M.-P., 1984a. *Handbook of Cenozoic Calcareous Nannoplankton* (Volume 1): *Orthoilithae (Discoasters)*: Flushing, NY (Micropaleontology Press).

Aubry, M.-P., 1984b. *Handbook of Cenozoic Calcareous Nannoplankton* (Volume 1): *Ortholithae (Holococcoliths, Ceratoliths, Ortholiths, and Others)*: Flushing, NY (Micropaleontology Press).

Aubry, M.-P., 1984c. *Handbook of Cenozoic Calcareous Nannoplankton* (Volume 1): *Ortholithae (Pentaliths and Others), Heliolithae (Fasciculiths, Sphenoliths, and Others)*: Flushing, NY (Micropaleontology Press).

Backman, J., and Raffi, I., 1997. Calibration of Miocene nannofossil events to orbitally tuned cyclostratigraphies from Ceara Rise. *In* Shackleton, N.J., Curry, W.B., Richter, C., and Bralower, T.J. (Eds.), *Proceedings of the Ocean Drilling Program, Scientific Results,* 154: College Station, TX (Ocean Drilling Program), 83–99. **https://doi.org/10.2973/odp.proc.sr.154.101.1997**

Backman, J., Raffi, I., Rio, D., Fornaciari, E., and Pälike, H., 2012. Biozonation and biochronology of Miocene through Pleistocene calcareous nannofossils from low and middle latitudes. *Newsletters on Stratigraphy,* 45(3):221–244. **https://doi.org/10.1127/0078-0421/2012/0022**

Backman, J., and Shackleton, N.J., 1983. Quantitative biochronology of Pliocene and early Pleistocene calcareous nannofossils from the Atlantic, Indian and Pacific Oceans. *Marine Micropaleontology,* 8(2):141–170. **https://doi.org/10.1016/0377-8398(83)90009-9**

Bown, P.R. (Ed.), 1998. *Calcareous Nannofossil Biostratigraphy:* London (Chapman and Hall).

Bown, P.R., and Young, J.R., 1998. Techniques. *In* Bown, P.R. (Ed.), *Calcareous Nannofossil Biostratigraphy:* Dordrecht, The Netherlands (Kluwer Academic Publishing), 16–28.

Doyongan, Y.I.L., and Fernando, A.G.S., 2021. Supplementary material, **https://doi.org/10.14379/iodp.proc.363.204supp.2021**. *Supplement to* Doyongan, Y.I.L., and Fernando, A.G.S., 2021. Data report: refinement of calcareous nannofossil biostratigraphy from the late Oligocene to the Pleistocene, IODP Expedition 363 Hole U1490A. *In* Rosenthal, Y., Holbourn, A.E., Kulhanek, D.K., and the Expedition 363 Scientists, *Western Pacific Warm Pool*. Proceedings of the International Ocean Discovery Program, 363: College Station, TX (International Ocean Discovery Program). https://doi.org/10.14379/iodp.proc.363.204.2021

Fornaciari, E., and Rio, D., 1996. Latest Oligocene to early middle Miocene quantitative calcareous nannofossil biostratigraphy in the Mediterranean region. *Micropaleontology*, 42(1):1–36. **https://doi.org/10.2307/1485981**

Gartner, S., 1977. Calcareous nannofossil biostratigraphy and revised zonation of the Pleistocene. *Marine Micropaleontology*, 2:1–25. **https://doi.org/10.1016/0377-8398(77)90002-0**

Martini, E., 1971. Standard Tertiary and Quaternary calcareous nannoplankton zonation. *In* Farinacci, A. (Ed.), *Proceedings of the Second Planktonic Conference, Roma 1970:* Rome (Edizioni Tecnoscienza), 2:739–785.

Okada, H., and Bukry, D., 1980. Supplementary modification and introduction of code numbers to the low-latitude coccolith biostratigraphic zonation (Bukry, 1973; 1975). *Marine Micropaleontology,* 5:321–325. **https://doi.org/10.1016/0377-8398(80)90016-X**

Olafsson, G., 1989. Quantitative calcareous nannofossil biostratigraphy of upper Oligocene to middle Miocene sediment from ODP Hole 667A and middle Miocene sediment from DSDP Site 574. *In* Ruddiman, W., Sarnthein, M., et al., *Proceedings of the Ocean Drilling Program, Scientific Results*, 108: College Station, TX (Ocean Drilling Program), 9–22. **https://doi.org/10.2973/odp.proc.sr.108.121.1989**

Perch-Nielsen, K., 1985. Cenozoic calcareous nannofossils. *In* Bolli, H.M., Saunders, J.B., and Perch-Nielsen, K. (Eds.), *Plankton Stratigraphy:* Cambridge, United Kingdom (Cambridge University Press), 427–554.

Raffi, I., Agnini, C., Backman, J., Catanzariti, R., and Pälike, H., 2016. A Cenozoic calcareous nannofossil biozonation from low and middle latitudes: a synthesis. *Journal of Nannoplankton Research*, 36(2):121–132.

Raffi, I., Backman, J., Fornaciari, E., Pälike, H., Rio, D., Lourens, L., and Hilgen, F., 2006. A review of calcareous nannofossil astrobiochronology encompassing the past 25 million years. *Quaternary Science Reviews,* 25(23–24):3113–3137. **https://doi.org/10.1016/j.quascirev.2006.07.007**

Raffi, I., Backman, J., and Rio, D., 1998. Evolutionary trends of tropical calcareous nannofossils in the late Neogene. *Marine Micropaleontology,* 35(1–2):17–41. **https://doi.org/10.1016/S0377-8398(98)00014-0**

Raffi, I., Backman, J., Rio, D., and Shackleton, N.J., 1993. Plio–Pleistocene nannofossil biostratigraphy and calibration to oxygen isotope stratigraphies from Deep Sea Drilling Project Site 607 and Ocean Drilling Program Site 677. *Paleoceanography,* 8(3):387–408. **https://doi.org/10.1029/93PA00755**

Raffi, I., and Flores, J.-A., 1995. Pleistocene through Miocene calcareous nannofossils from eastern equatorial Pacific Ocean (Leg 138). *In* Pisias, N.G., Mayer, L.A., Janecek, T.R., Palmer-Julson, A., and van Andel, T.H. (Eds.), *Proceedings of the Ocean Drilling Program, Scientific Results,* 138: College Station, TX (Ocean Drilling Program), 233–286. **https://doi.org/10.2973/odp.proc.sr.138.112.1995**

Raffi, I., Rio, D., d'Atri, A., Fornaciari, E., and Rocchetti, S., 1995. Quantitative distribution patterns and biomagnetostratigraphy of middle and late Miocene calcareous nannofossils from equatorial Indian and Pacific Oceans (Legs 115, 130, and 138). *In* Pisias, N.G., Mayer, L.A., Janecek, T.R., Palmer-Julson, A., and van Andel, T.H. (Eds.), *Proceedings of the Ocean Drilling Program, Scientific Results*, 138: College Station, TX (Ocean Drilling Program), 479–502. **https://doi.org/10.2973/odp.proc.sr.138.125.1995**

Rio, D., Raffi, I., and Villa, G., 1990. Pliocene–Pleistocene calcareous nannofossil distribution patterns in the western Mediterranean. *In* Kastens, K.A., Mascle, J., et al., *Proceedings of the Ocean Drilling Program, Scientific Results,* 107: College Station, TX (Ocean Drilling Program), 513–533. **https://doi.org/10.2973/odp.proc.sr.107.164.1990**

Rosenthal, Y., Holbourn, A.E., Kulhanek, D.K., Aiello, I.W., Babila, T.L., Bayon, G., Beaufort, L., Bova, S.C., Chun, J.-H., Dang, H., Drury, A.J., Dunkley Jones, T., Eichler, P.P.B., Fernando, A.G.S., Gibson, K.A., Hatfield, R.G., Johnson, D.L., Kumagai, Y., Li, T., Linsley, B.K., Meinicke, N., Mountain, G.S., Opdyke, B.N., Pearson, P.N., Poole, C.R., Ravelo, A.C., Sagawa, T., Schmitt, A., Wurtzel, J.B., Xu, J., Yamamoto, M., and Zhang, Y.G., 2018a. Expedition 363 methods. *In* Rosenthal, Y., Holbourn, A.E., Kulhanek, D.K., and the Expedition 363 Scientists, *Western Pacific Warm Pool.* Proceedings of the International Ocean Discovery Program, 363: College Station, TX (International Ocean Discovery Program). **https://doi.org/10.14379/iodp.proc.363.102.2018**

Rosenthal, Y., Holbourn, A.E., Kulhanek, D.K., Aiello, I.W., Babila, T.L., Bayon, G., Beaufort, L., Bova, S.C., Chun, J.-H., Dang, H., Drury, A.J., Dunkley Jones, T., Eichler, P.P.B., Fernando, A.G.S., Gibson, K.A., Hatfield, R.G., Johnson, D.L., Kumagai, Y., Li, T., Linsley, B.K., Meinicke, N., Mountain, G.S., Opdyke, B.N., Pearson, P.N., Poole, C.R., Ravelo, A.C., Sagawa, T., Schmitt, A., Wurtzel, J.B., Xu, J., Yamamoto, M., and Zhang, Y.G., 2018b. Expedition 363 summary. *In* Rosenthal, Y., Holbourn, A.E., Kulhanek, D.K., and the Expedition 363 Scientists, *Western Pacific Warm Pool.* Proceedings of the International Ocean Discovery Program, 363: College Station, TX (International Ocean Discovery Program). **https://doi.org/10.14379/iodp.proc.363.101.2018**

Rosenthal, Y., Holbourn, A.E., Kulhanek, D.K., Aiello, I.W., Babila, T.L., Bayon, G., Beaufort, L., Bova, S.C., Chun, J.-H., Dang, H., Drury, A.J., Dunkley Jones, T., Eichler, P.P.B., Fernando, A.G.S., Gibson, K.A., Hatfield, R.G., Johnson, D.L., Kumagai, Y., Li, T., Linsley, B.K., Meinicke, N., Mountain, G.S., Opdyke, B.N., Pearson, P.N., Poole, C.R., Ravelo, A.C., Sagawa, T., Schmitt, A., Wurtzel, J.B., Xu, J., Yamamoto, M., and Zhang, Y.G., 2018c. Site U1490. *In* Rosenthal, Y., Holbourn, A.E., Kulhanek, D.K., and the Expedition 363 Scientists, *Western Pacific Warm Pool*. Proceedings of the International Ocean Discovery Program, 363: College Station, TX (International Ocean Discovery Program). **https://doi.org/10.14379/iodp.proc.363.111.2018**

Thierstein, H.R., Geitzenauer, K.R., Molfino, B., and Shackleton, N.J., 1977. Global synchroneity of late Quaternary coccolith datum levels validation by oxygen isotopes. *Geology,* 5(7):400–404. **https://doi.org/10.1130/0091-7613(1977)5<400:GSOLQC>2.0.CO;2**

Young, J.R., 1991. A Quaternary nannofossil range chart. *International Nannoplankton Association Newsletter*, 13:14–17. **http://ina.tmsoc.org/JNR/NINAarticles/Young%201991%20INANewsl%2013(1)%20Q%20zonation%20[%C2%A7N2007].pdf**

Young, J.R., Bown, P.R., and Lees, J.A., 2017. Nannotax3. **http://www.mikrotax.org/Nannotax3/**

Appendix

Species list

Amaurolithus Gartner and Bukry, 1975
Amaurolithus brevigracilis de Kaenel and Bergen, in de Kaenel et al., 2017
Amaurolithus delicatus Gartner and Bukry, 1975
Amaurolithus primus (Bukry and Percival, 1971) Gartner and Bukry, 1975
Calcidiscus leptoporus (Murray and Blackman, 1898) Loeblich and Tappan, 1978
Calcidiscus macintyrei (Bukry and Bramlette, 1969) Loeblich and Tappan, 1978
Calcidiscus premacintyrei Theodoridis, 1984
Calcidiscus salomonii da Gama and Varol, 2013
Calcidiscus tropicus Kamptner, 1956 sensu Gartner, 1992
Catinaster calyculus Martini and Bramlette, 1963
Catinaster coalitus Martini and Bramlette, 1963
Ceratolithus apiculus de Kaenel and Bergen, in de Kaenel et al., 2017
Ceratolithus armatus Müller, 1974
Ceratolithus cristatus Kamptner, 1950
Ceratolithus larrymayeri Backman and Raffi, in Raffi et al., 1998
Coccolithus miopelagicus Bukry, 1971
Coccolithus pelagicus (Wallich, 1871) Schiller, 1930
Coronocyclus baileyi da Gama and Varol, 2013
Coronocyclus mesostenos de Kaenel and Boesiger, in Boesiger et al., 2017
Coronocyclus nitescens (Kamptner, 1963) Bramlette and Wilcoxon, 1967
Cryptococcolithus mediaperforatus (Varol, 1991) de Kaenel and Villa, 1996
Cyclicargolithus abisectus (Muller, 1970) Wise, 1973
Cyclicargolithus floridanus (Roth and Hay, in Hay et al., 1967) Bukry, 1971
Discoaster asymmetricus Gartner, 1969
Discoaster bellus Bukry and Percival, 1971
Discoaster berggrenii Bukry, 1971
Discoaster braarudii Bukry, 1971
Discoaster brouweri Tan, 1927
Discoaster calcaris Gartner, 1967
Discoaster decorus (Bukry, 1971) Bukry, 1973
Discoaster deflandrei Bramlette and Riedel, 1954
Discoaster exilis Martini and Bramlette, 1963
Discoaster hamatus Martini and Bramlette, 1963
Discoaster pansus (Bukry and Percival, 1971) Bukry, 1973
Discoaster pentaradiatus Tan, 1927
Discoaster quinqueramus Gartner, 1969
Discoaster surculus Martini and Bramlette, 1963
Discoaster tamalis Kamptner, 1967
Discoaster triradiatus Tan, 1927
Discoaster variabilis Martini and Bramlette, 1963
Emiliania huxleyi (Lohmann, 1902) Hay and Mohler, in Hay et al., 1967
Gephyrocapsa Kamptner, 1943
Gephyrocapsa caribbeanica Boudreaux and Hay, in Hay et al., 1967
Gephyrocapsa oceanica Kamptner, 1943
Hayaster perplexus (Bramlette and Riedel, 1954) Bukry, 1973
Helicosphaera ampliaperta Bramlette and Wilcoxon, 1967
Helicosphaera carteri (Wallich, 1877) Kamptner, 1954
Helicosphaera euphratis Haq, 1966
Helicosphaera intermedia Martini, 1965
Helicosphaera sellii (Bukry and Bramlette, 1969) Jafar and Martini, 1975
Helicosphaera stalis Theodoridis, 1984
Helicosphaera wallichii (Lohmann, 1902) Okada and McIntyre, 1977
Nicklithus amplificus (Bukry and Percival, 1971) Raffi, Backman, and Rio, 1998
Orthorhabdus rugosus (Bramlette and Wilcoxon, 1967) Young and Bown, 2014
Pontosphaera Lohmann, 1902
Pseudoemiliania lacunosa (Kamptner, 1963) Gartner, 1969
Reticulofenestra asanoi Sato and Takayama, 1992
Reticulofenestra haqii Backman, 1978
Reticulofenestra minuta Roth, 1970
Reticulofenestra minutula (Gartner, 1967) Haq and Berggren, 1978
Reticulofenestra perplexa (Burns, 1975) Wise, 1983
Reticulofenestra pseudoumbilicus (Gartner, 1967) Gartner, 1969
Rhabdosphaera clavigera Murray and Blackman, 1898
Scyphosphaera Lohmann, 1902
Sphenolithus Deflandre, in Grassé, 1952
Sphenolithus abies Deflandre, in Deflandre and Fert, 1954
Sphenolithus apoxis Bergen and de Kaenel, in Bergen et al., 2017
Sphenolithus belemnos Bramlette and Wilcoxon, 1967
Sphenolithus bipedis Bergen and de Kaenel, in Bergen et al., 2017
Sphenolithus calyculus Bukry, 1985
Sphenolithus conicus Bukry, 1971
Sphenolithus delphix Bukry, 1973
Sphenolithus disbelemnos Fornaciari and Rio, 1996
Sphenolithus dissimilis Bukry and Percival, 1971
Sphenolithus heteromorphus Deflandre, 1953
Sphenolithus microdelphix Bergen and de Kaenel, in Bergen et al., 2017
Sphenolithus moriformis (Bronnimann and Stradner, 1960) Bramlette and Wilcoxon, 1967
Sphenolithus procerus Maiorano and Monechi, 1997
Sphenolithus puniceus Bergen and de Kaenel, in Bergen et al., 2017
Sphenolithus spiniger Bukry, 1971
Sphenolithus spinula Bergen and de Kaenel, in Bergen et al., 2017
Triquetrorhabdulus carinatus Martini, 1965
Umbilicosphaera sibogae (Weber-van Bosse, 1901) Gaarder, 1970